

Research Paper

Uptake and Transport of PEG-Graft-Trimethyl-Chitosan Copolymer–Insulin Nanocomplexes by Epithelial Cells

Shirui Mao,^{1,2} Oliver Germershaus,¹ Dagmar Fischer,¹ Thomas Linn,³ Robert Schnepf,⁴ and Thomas Kissel^{1,5}

Received April 30, 2005; accepted August 16, 2005

Purpose. The effect of chitosan and polyethylene glycol (PEG)ylated trimethyl chitosan copolymer structure on the uptake and transport of insulin nanocomplexes was evaluated and transport mechanisms were investigated.

Methods. Insulin nanocomplexes were prepared from chitosan and its copolymers by self-assembly. Complex uptake in Caco-2 cells was quantified by measuring the cell-associated fluorescence and cellular localization was visualized by confocal laser scanning microscopy (CLSM) using tetra-methyl-rhodamine isothiocyanate-labeled insulin. The transport of selected insulin complexes through Caco-2 monolayers was then investigated and compared with *in vivo* uptake by nasal epithelium in diabetic rats.

Results. All complexes were 200–400 nm in diameter, positively charged, and displayed an insulin loading efficiency of approximately 90%. *In vitro* release of insulin from the complexes was dependent on the medium pH. Insulin uptake was enhanced by nanocomplex formation, and was dependent on incubation time, temperature, and concentration. Complex uptake in Caco-2 cells was inhibited by 25.2 ± 1.3%, 13.0 ± 1.0%, and 16.6 ± 0.7% in the presence of cytochalasin D, sodium azide, and 2,4-dinitrophenol, respectively. The uptake mechanism was assumed to be adsorptive endocytosis. Additionally, cell uptake efficiency was shown to be influenced by a combination of polymer molecular weight, viscosity, and positive charge density. However, none of the nanocomplexes displayed improved transport properties when compared to insulin transport data after 2 h incubation with Caco-2 monolayers. This result was further confirmed with animal experiments.

Conclusions. Small, stable insulin nanocomplexes were formed using PEGylated trimethyl chitosan copolymers, which significantly enhanced the uptake of insulin in Caco-2 cells by adsorptive endocytosis. However, nanocomplexation did not seem to enhance transcellular insulin transport across cell monolayers, which is in line with animal data in rats. This implies that PEGylated trimethyl chitosan complexes with insulin need further optimization and the Caco-2 cell line is a predictable *in vitro* cell culture model for drug absorption.

KEY WORDS: Caco-2 cells; insulin nanocomplexes; PEGylation; trimethyl chitosan; uptake.

INTRODUCTION

To maintain blood glucose levels at a near-physiological level and thereby minimize long-term diabetic complications, treatment of insulin-dependent diabetes requires up to four subcutaneous injections per day. To circumvent this tedious regimen of therapy, several attempts have been made to exploit mucosal surfaces for the delivery of macromolecular drugs, especially the nasal, pulmonary, and oral mucosae (1).

The nasal route has been a particular focus of recent research as biologically active peptides, such as desmopressin, salmon calcitonin, and corticotrophin, show significant absorption across the nasal mucosa (2).

In fact, the nasal route has been recognized as an attractive alternative to parenteral administration of insulin since 1922 (3). Despite the promise of intranasal administration for the delivery of peptides, the efficacy of the nasal route for the absorption of large peptides, e.g., insulin, is relatively low (4). Therefore, new nasal delivery systems enhancing insulin absorption have been proposed, including surfactants, protease inhibitors, and bioadhesive polymers or microspheres (5,6). Unfortunately, most penetration enhancers such as surfactants, bile salts, and fatty acids cause irreversible damage, or irritation to the nasal mucosa when used at efficacious concentrations (7). By contrast, bioadhesive nanoparticles and microparticles have been demonstrated to be well-tolerated macromolecular carriers (8,9).

Chitosan, a nontoxic and biocompatible cationic polysaccharide produced by partial deacetylation of chitin

¹ Department of Pharmaceutics and Biopharmacy, Philipps-University of Marburg, Ketzlerbach 63, D-35032 Marburg, Germany.

² College of Pharmacy, Shenyang Pharmaceutical University, Wenhua Road 103, 110016 Shenyang, China.

³ Medical Clinic III and Policlinic, Justus Liebig University, Rodthohl 6, D-35385 Giessen, Germany.

⁴ Complex Biosystems, Im Neuenheimer Feld 584, D-69120 Heidelberg, Germany.

⁵ To whom correspondence should be addressed. (e-mail: kissel@mail.uni-marburg.de)

derived from naturally occurring crustacean shells, was reported to reversibly open tight junctions. The use of chitosan as a nasal delivery system was reviewed recently (10). Intranasal administration of chitosan insulin nanoparticles, formed by a mild ionotropic gelation procedure, enhanced the nasal absorption of insulin to a greater extent than an aqueous solution of chitosan (11). On the other hand, Dyer *et al.* (12) showed that chitosan nanoparticles did not improve the absorption-enhancing effect of chitosan in solution or powder form and that chitosan powder was the most effective formulation for the nasal delivery of insulin in a sheep model. These discrepancies cast some doubts on the advantage of nanoparticulate carriers for intranasal administration of insulin.

The mechanism of action of chitosan was attributed to be a combination of bioadhesion and a transient opening of tight junctions between epithelial cells (13). However, this absorption enhancing ability was evident only under acidic conditions (pH < 6.5), where most of the amino groups were protonated.

To overcome this problem, polyethylene glycol (PEG)-ylated trimethyl chitosan copolymers were synthesized in our laboratory in an attempt to increase the solubility of chitosan at physiological pH and improve the biocompatibility of trimethyl chitosan (TMC) (14). Insulin nanocomplexes were prepared with the copolymers by electrostatic interaction. We speculated that by combining absorption enhancer properties (chitosan) with nanoscale dimensions (complexes), intranasal absorption of insulin could potentially be improved.

The goal of this study was to evaluate the effect of chitosan and PEGylated TMC copolymer structure on the uptake and transport of insulin nanocomplexes, and elucidate their mechanism of transport. For mechanistic studies, Caco-2, a human colon adenocarcinoma cell line, was used as *in vitro* cell culture model to investigate particle uptake (15,16). Such monolayers formed tight junctions, and exhibited barrier properties similar to those in intestinal and nasal epithelia. The predictive power of cell culture experiments with Caco-2 monolayers was further assessed in animal studies.

MATERIALS AND METHODS

Polymers

Chitosan (400 kDa) was purchased from Fluka (Steinheim, Germany) with a degree of deacetylation (DD) of 84.7% and depolymerized by oxidative degradation to yield chitosan with molecular weights of ca. 100 and 50 kDa (17). PEGylated TMC copolymers were synthesized as described elsewhere (14). Briefly, TMC dissolved in purified water (10 mg/mL) and *N*-hydroxysuccinimide (NHS)-mPEG dissolved in dry DMSO (50 mg/mL) were mixed and stirred at room temperature for 24 h. Then the solution was purified by ultrafiltration twice using an Amicon cell equipped with a 10,000-MW (molecular weight) cutoff membrane. The dialyzed solution was finally freeze-dried. The number of PEG chains grafted per TMC macromolecule (graft ratio) was calculated from integrals of the ¹H NMR signals for PEG blocks at ~3.35 ppm (–OCH₃) and TMC blocks at ~3.0 ppm (–N(CH₃)₂) and ~3.3 ppm (–N⁺(CH₃)₃), using the known

molecular weight of mPEG. The graft ratio (wt%) was calculated according to the following equation:

$$\text{Graft ratio (wt\%)} = \frac{MW_{\text{PEG}} * n}{(MW_{\text{PEG}} * n + MW_{\text{TMC}})}$$

where MW_{PEG} is the molecular weight of PEG, MW_{TMC} is the molecular weight of TMC, and *n* is the average number of PEG chains per TMC macromolecule calculated by ¹H NMR.

The following nomenclature was adopted for the copolymers: PEG(*X*)_{*n*}-g-TMC(*Y*), where *X* denotes the molecular weight (MW) of polyethylene glycol (PEG) in Da, *Y* denotes the MW of TMC in kDa, and the subscript *n* represents the average number of PEG chains per TMC macromolecule of *Y* kDa.

Preparation and Characterization of Copolymer-Insulin Self-Assembled Nanocomplexes

The complexes were prepared by self-assembly, utilizing the electrostatic interactions between the positively charged polymers and negatively charged insulin (Aventis Pharma AG, Frankfurt, Germany) as a driving force. Briefly, nanocomplexes were prepared by mixing equal volumes of insulin and polymer solution at the desired ratio (Table I) under gentle magnetic stirring, and incubated for a further 20 min at room temperature. For the preparation of chitosan-insulin complex, the pH of chitosan solution was adjusted to 5.5 and the pH of insulin solution was 8.5. In contrast, for the preparation of TMC and copolymer-insulin complex, the polymer solution and insulin solution were adjusted to pH 7.5. Complex sizes and zeta potentials were obtained using dynamic light scattering (DLS) and laser Doppler anemometry (LDA) measurements.

Dynamic Light Scattering. Complex size measurements were carried out with a Zetasizer 3000 HS from Malvern Instruments (Herrenberg, Germany; 10 mW HeNe laser, 633 nm). Scattering light was detected at a 90° angle through a 400-μm pin hole at a temperature of 25°C. Kcps (kilo counts per second), which is a measure of nanocomplexes concentration in a sample, was recorded during the measurement. Particle sizes of polyelectrolyte complexes (PEC) are given as mean ± SD (*n* = 10).

Laser Doppler Anemometry. The zeta potential measurements of the complexes were carried out in the standard capillary electrophoresis cell of the Zetasizer 3000 HS from Malvern Instruments (Herrenberg, Germany) at 25°C in 0.01 M Tris buffer pH 7.4 except chitosan (0.01 M Tris buffer pH 6.8). Average values of the zeta potential were calculated with the data from ten runs (±SD).

In Vitro Release Studies

Insulin release was determined by incubating the complexes (100 μL) in 1.5 mL Tris buffer (pH 7.4) and acetate buffer (pH 4.0) at 37°C. The concentration of the complex in the release media was adjusted to maintain sink conditions for insulin. At appropriate time intervals (30 min, 45 min, 1 h, 2 h, 4 h, and 6 h) individual samples were centrifuged at 14,000 rpm/min for 30 min and the amount of insulin released from the complexes was evaluated by high-performance liquid chromatography as described elsewhere (18).

Table I. Properties and Characteristics of the Polymers and Their Nanocomplexes with Insulin

Polymers (kDa)	DD (%) ^a	Substitution (%) ^b	Graft ratio (%) ^c	IC ₅₀ (3 h) (µg/mL)	Mass ratio ^d	Size (nm)	ξ (mV)	Association efficiency (%)	Charge ratio (polymer/insulin)
Chitosan, 400	85.1			>500	2:1	376.4 ± 10.3	13.6 ± 0.3	89.7 ± 2.1	7:1
Chitosan, 100	85.4			>500	2:1	308.2 ± 8.5*	8.8 ± 0.4	87.3 ± 2.4	7:1
Chitosan, 50	86.2			>500	2:1	226.8 ± 6.3*	7.4 ± 0.3	93.2 ± 1.3	7:1
TMC, 100		39.3 ^e		70	0.3:1	273.3 ± 4.6	19.8 ± 1.1	81.4 ± 2.1	3:1
TMC, 50		39.6 ^e		90	0.3:1	236.6 ± 1.3	21.4 ± 0.3	86.3 ± 3.2	3:1
PEG(5k) ₄₀ -g-TMC(100)		6.44	66.1 ± 2.2	>500	1:1	233.3 ± 7.2	18.8 ± 0.3	94.8 ± 1.1	5:1
PEG(550) ₂₂₈ -g-TMC(100)		36.7	58.5 ± 3.1	>500	1:1	224.6 ± 2.3	13.9 ± 2.9**	94.2 ± 1.7	5:1
PEG(5k) ₁₉ -g-TMC(50)		6.13	64.9 ± 1.7	>500	1:1	203.9 ± 7.2	15.0 ± 1.2**	90.4 ± 4.4	5:1
PEG(550) ₁₃₂ -g-TMC(50)		37.4	59.2 ± 3.0	>500	1:1	220.3 ± 5.5	16.4 ± 1.9**	94.7 ± 3.3	5:1

^a Degree of deacetylation, calculated by ¹H NMR analysis.

^b Calculated based on the primary amino group content in chitosan.

^c Calculated based on the composition of the copolymer by ¹H NMR analysis.

^d Optimized polymer/insulin mass ratio for preparation of complexes.

^e Degree of quaternization.

*Particle size decreased significantly ($p < 0.05$) compared with that of chitosan (400 kDa)–insulin nanocomplexes.

**Zeta potential decreased significantly ($p < 0.05$) compared with that of TMC (100 and 50 kDa)–insulin nanocomplexes.

Labeling of Polymers and Insulin

Chitosan (100 kDa), PEG(5k)₄₀-g-TMC(100), and PEG(5k)₁₉-g-TMC(50) were labeled with Oregon Green carboxylic acid succinimidyl ester (Oregon Green 488; Molecular Probes, Eugene, OR, USA) following a previously described method (19). Insulin was labeled with tetra-methyl-rhodamine isothiocyanate (TRITC; Sigma, Taufkirchen, Germany). Briefly, insulin was dissolved at a concentration of 4.5 mg/mL in 0.1 M sodium bicarbonate buffer (pH 9.3). A solution of TRITC (1 mg/mL) in dimethyl sulfoxide (DMSO) was added dropwise under stirring (insulin/TRITC molar ratio = 1:2.9) and the mixture was stirred for 18 h at 4°C under light exclusion. The reaction was quenched with an excess of ammonium chloride, and stirred for a further 4 h. Purification was performed on a PD-10 desalting column (Amersham Pharmacia Biotech, Freiburg, Germany) with phosphate-buffered salt (PBS) solution (pH 7.4).

Cell Culture

Mycoplasma-free Caco-2 cells were used at passage numbers 44–50 (HD, DKFZ, German Cancer Research Institute, Heidelberg, Germany) under previously described conditions (20). Cells were seeded at a density of 6×10^4 cells/cm² on 12-well cell culture plates or 6-well uncoated polycarbonate Transwell™ filter inserts (Costar, Bodenheim, Germany; 0.4 µm pore size, area: 4.71 cm²) and cultivated over 21 days. The medium was changed every second day.

MTT Assay

In vitro cytotoxicity of the polymers was evaluated using an MTT assay with L929 fibroblast cell line, as described previously (17). Briefly, L929 cells were seeded into 96-well microtiter plates at a density of 8000 cells/well. After 24 h,

the culture medium was replaced with 100-µL serial dilutions of polymer and cells were incubated for a further 3 h. Subsequently, 20 µL 3-(4,5-dimethyl-thiazol-2-yl)-2,5-diphenyl tetrazolium bromide (MTT) (5 mg/mL) was added to each well. After 4 h incubation, unreacted dye was aspirated and the formazan crystals were dissolved in DMSO (200 µL/well). Absorption was measured at 570 nm with a background correction of 690 nm using a Titertek Plus MS 212 ELISA reader (ICN, Eschwege, Germany). The relative cell viability compared to control cells containing cell culture medium (pH 6.5) without polymer was calculated by $[A]_{\text{test}} / [A]_{\text{control}}$. IC₅₀ (the concentration at which cell growth is inhibited by 50%) values were calculated.

Uptake Studies

Cell uptake studies were performed with Caco-2 cell monolayers according to the method described by Behrens *et al.* (21). The uptake medium was 0.01 M Tris buffer, supplemented with 100 mM glucose, 1.17 mM CaCl₂, 1.03 mM MgCl₂, pH 7.4. The cell lysate, obtained by solubilizing the cells with 300 µL/well 2% SDS (pH 8.0), was measured for fluorescence with an LS 50B spectrometer (Perkin Elmer, Ueberlingen, Germany) at an excitation wavelength of 543 nm and an emission wavelength of 560 nm. Protein content was determined via bicinchoninic acid (BCA) assay according to the manufacturer's protocol (Promega, Mannheim, Germany). Uptake was expressed as the quantity of insulin associated with 1 mg of cellular protein (mean ± SD, $n = 3$). With PEG(5k)₄₀-g-TMC(100) copolymer–insulin complex, the effect of polymer concentration, incubation time, insulin concentration, and temperature on complex uptake was investigated. To further evaluate the possibility of complex uptake occurring through an active process, cells were preincubated with the metabolic inhibitors sodium azide (10 mM) and 2,4-dinitrophenol (0.2 mM), endocytosis inhibitors cytochalasin D (0.1 µg/mL), and noco-

dazole (1 µg/mL) (all were obtained from Sigma, Steinheim, Germany) for 30 min prior to complex application and throughout the 2-h uptake experiment.

Confocal Laser Scanning Microscopy

CLSM was utilized to visualize the internalization of insulin nanocomplexes. Caco-2 cells grown on glass cover slips for 7 days were treated with insulin, polymers, and complexes (insulin concentration = 250 µg/mL). After 2 h incubation at 37°C, cells were washed three times with ice-cold transport buffer, fixated with 3.7% paraformaldehyde in PBS (pH 7.4) at room temperature for 30 min, and counterstained with 4,6-diamidino-2-phenylindole (DAPI; 0.2 µg/mL) for 20 min, both under light exclusion. For samples without labeled polymer, cells were counterstained with fluorescein isothiocyanate (FITC)-labeled wheat germ agglutinin (WGA; 0.01 µg/mL) for 30 min. Samples were embedded in Fluor-Save™ Reagent (Calbiochem, Darmstadt, Germany) and imaged via CLSM (Zeiss Axiovert 100 M Microscope coupled to a Zeiss LSM 510 scanning device; Jena, Germany), which was equipped with a Zeiss Neofluor 63*/1.2 objective. Excitation wavelengths were 364 nm [long pass (LP) filter, 385 nm] for DAPI, 488 nm (LP 505 nm) for Oregon Green 488 and FITC, and 543 nm (LP 567 nm) for TRITC (18,20). All images were recorded using the multitracking mode, in which each fluorescence channel was scanned individually. Additionally, trypan blue was postincubated with cells for 1 min (400 µg/mL in 0.1 M citrate buffer, pH 4.4) after 2 h incubation with the complexes or polymers.

Transport Across Caco-2 Cell Monolayers

Transport studies were performed 21 days postseeding. The integrity of the monolayers was checked by measuring the transepithelial electrical resistance (TEER) values in Hank's balanced salt solution (HBSS; pH 7.4) buffer before and after the experiment, as described previously (20,21). Only cells with TEER values in the range of 250–350 Ω · cm² were used for the transport studies. Briefly, filter inserts were rinsed with transport buffer (pH 7.4) (the same as the uptake medium) and allowed to equilibrate at 37°C for 15 min. Experiments were carried out by replacing the apical buffer (1.5 mL) with the samples (insulin 250 µg/mL) and the basolateral buffer with fresh transport buffer (2.5 mL). Every 20 min up to 2 h, a 1.0-mL sample was collected from the basolateral chamber and replaced with fresh buffer. Each experiment was performed in triplicate. To study TEER reversibility, monolayers were rinsed with fresh transport buffer directly after the transport experiment and allowed to regenerate in fresh culture medium under culture conditions. After 24 h, monolayer integrity was checked in HBSS buffer.

Calculations and Statistics

The apparent permeability coefficient (P_{eff} , cm/s) was calculated using the following equation:

$$P_{\text{eff}} = \frac{V_R}{AC_0} \frac{dc}{dt}$$

where dc/dt (µg/s) represents the time derivative of concentration in the receiver chamber, A (cm²) the surface area of the monolayer, V_R (cm³) the volume of the receiver chamber, and C_0 (µg) the initial concentration in the apical compartment. The quantity of all cell-associated insulin was calculated by subtracting the amounts transported and remaining in the apical compartment from the initial amount. Results were expressed as mean value ± SD of three experiments. Significance between the mean values was calculated using one-way ANOVA analysis (Origin 7.0 SRO, Northampton, MA, USA). Probability values (p) less than 0.05 were considered significant.

Animal Experiment

Male Wistar rats of about 250 g (Charles River, Wiga, Germany) were fasted overnight with free access to water. Diabetic rats were obtained after streptozotocin treatment (55 mg/kg) and included into the experiment when blood glucose levels exceeded 250 mg/dL. Rats were anesthetized by ether inhalation for ~2 min in a sealed glass container, followed by intraperitoneal injection of Avertin. The animals were dosed at 10 µL/g body weight and remained anesthetized for 60–90 min (healthy) and 30–40 min (diabetic) in a supine position. The following formulations were administered intranasally: (1) control insulin solution (insulin dose, 5 U/kg); (2) PEG(5k)₄₀-g-TMC(100) insulin nanocomplex suspension (pH 7.4; insulin dose, 5 U/kg). They were carefully delivered to the right nostril (~20 µL) only, using a Hamilton syringe with an attached polyethylene tube, which was inserted about 0.5 cm into the nostril. Blood glucose levels were measured directly in blood collected from the tip of the rat tail using a glucose meter (Glucometer Elite; Bayer Corp., Leverkusen, Germany) at the time points of -10 and -5 min before formulation application and at various time intervals up to 4 h postadministration. The values of the blood glucose baselines were in the range of 350–500 mg/dL for diabetic rats. Glucose concentration was calculated as a percentage of the mean value of the first three measurements for each animal. Mean values of plasma glucose levels (±SD) of four rats in each group and areas under curve were determined. Student's t test was performed to compare both experimental groups with GraphPad (San Diego, USA) software. The animal study was conducted according to the principles outlined in the *Guide for the Care and Use of Laboratory Animal Resources* (National Academy Press, Washington) and had received approval by the Animal Review Committee at the local authorities.

RESULTS AND DISCUSSION

Physicochemical Characteristics of Polymers and Complexes

The properties of the polymers and the self-assembled insulin nanocomplexes are summarized in Table I. All complexes showed a size in the range of 200–400 nm, a positive surface charge and insulin association efficiency (AE) of approximately 90%. The measured particle size of the complexes decreased with the molecular weight (MW) of chitosan ($p < 0.05$). The size of the copolymer-insulin complexes was comparable to that of 50 kDa chitosan and 50 kDa TMC. The zeta potential of chitosan-insulin complexes was approxi-

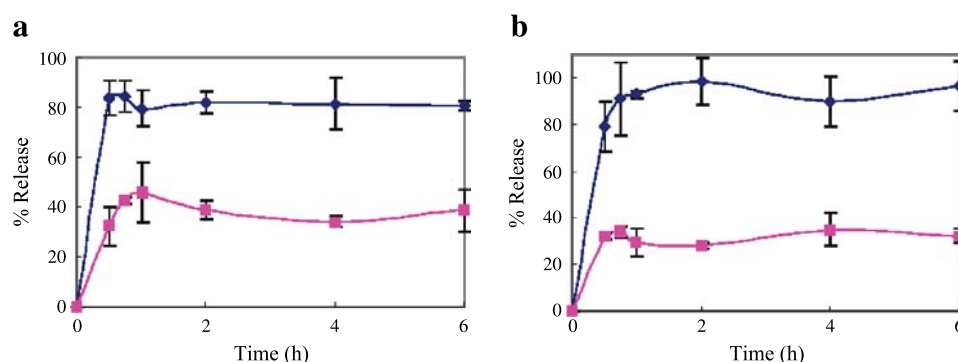


Fig. 1. *In vitro* release of insulin from complexes at different pH. (a) Chitosan (100 kDa)-insulin complexes. (b) PEG(5k)₄₀-g-TMC(100)-insulin complexes. (◆) pH 4.0, (■) pH 7.4.

mately 2-fold lower than that of TMC and copolymers, and a slightly or significantly decreased zeta potential was observed for the copolymers compared to that of TMC. With a similar graft ratio, the zeta potential of PEG(550)₂₂₈-g-TMC(100) copolymer was lower compared to that of PEG(5k)₄₀-g-TMC(100) due to the increased substitution ratio. The optimal charge ratio between polymer and insulin was polymer structure-dependent: it was 7:1 for chitosan, compared to 3:1 for TMC.

Figure 1 exemplifies the release profiles of insulin from complexes formed with chitosan (100 kDa) and PEG(5k)₄₀-g-TMC(100). Similar profiles were obtained for the two complexes, showing a pH-dependent insulin release. At pH 4.0, both chitosan and insulin were positively charged, rendering complexes dissociation due to electrostatic repulsion and therefore, complete insulin release. This is consistent with a previous report (11). In contrast, less than 40% insulin was released from the complex at pH 7.4 Tris buffer in 6 h, which was slow compared to the release of insulin from chitosan-insulin nanoparticles in phosphate buffer of pH 7.4, possibly due to interactions of phosphate ions with chitosan (22). Therefore, 0.01 M Tris buffer (pH 7.4) was selected for further studies.

Mechanism of Insulin Complexes Uptake

As shown in Fig. 1, after 2 h incubation at 37°C, approximately 40% of insulin was released from the complexes at pH 7.4 in Tris buffer. Therefore, insulin uptake in Caco-2 monolayers comprises both complex bound insulin and free insulin. Based on the results of uptake experiment (Fig. 5), the PEG(5k)₄₀-g-TMC(100) copolymer-insulin complex was selected for further studies as a carrier system. Properties of the

complexes were summarized in Table II. The complexes were stable at least for 4 h, which was sufficient for uptake studies.

The effect of polymer concentration, incubation time, insulin concentration, and temperature on uptake was investigated, and results are shown in Fig. 2. Insulin uptake increased with increasing polymer concentration. A 2.5-fold increase was measured when the polymer concentration increased from 125 to 500 µg/mL. Moreover, a linear relationship was established between uptake percentage and polymer concentration in the range studied (Fig. 2a). As shown in Fig. 2b, insulin uptake increased with incubation time, and more than 4-fold uptake was observed by prolonging the incubation time from 0.5 to 4 h. Moreover, the rate of uptake increased with insulin concentration despite the increased particle size, and decreased charge density (Table II) and did not exhibit saturation in the range of 62.5–500 µg/mL (Fig. 2c). The uptake amount increased 5-fold when the concentration increased from 62.5 to 500 µg/mL. However, the uptake efficiency decreased with increasing insulin concentration and leveled off at 250 µg/mL at 37°C (Fig. 2d). At 4°C the uptake efficiency was less than 3% irrespective of insulin concentration. Lowering the temperature from 37 to 4°C abolished uptake of insulin complexes by approximately 70%, indicating that the uptake is temperature-dependent. These results suggest that an energy-dependent endocytic process could be responsible for up to 70% of complexes uptake, and the other 30% attribute to physical adhesion or diffusion.

Effect of Inhibitors

When the complexes were preincubated with either sodium azide or 2,4-dinitrophenol for 30 min, complexes

Table II. Characteristics of PEG(5k)₄₀-g-TMC(100) Copolymer Insulin Nanocomplexes Used in Uptake Studies

No.	Polymer concentration (µg/mL)	Insulin concentration (µg/mL)	Particle size (nm)	Polydispersity index	Zeta potential (mV)	Association efficiency (%)
1	125	125	265.8 ± 3.9	0.26 ± 0.08	18.8 ± 0.3	94.8 ± 1.1
2	250	125	168.6 ± 9.5	0.38 ± 0.01	20.3 ± 1.3	92.9 ± 0.5
3	375	125	157.8 ± 4.8	0.36 ± 0.04	22.4 ± 2.4	74.3 ± 0.3
4	500	125	129.5 ± 2.1	0.36 ± 0.02	23.4 ± 3.3	60.9 ± 3.1
5	125	62.5	226.7 ± 10.8	0.43 ± 0.06	20.0 ± 2.1	92.9 ± 0.5
6	125	125	265.8 ± 3.9	0.26 ± 0.08	18.8 ± 0.3	94.8 ± 1.1
7	125	250	320.6 ± 8.3	0.41 ± 0.01	11.1 ± 1.8	91.8 ± 2.1
8	125	500	375.2 ± 10.7	0.27 ± 0.06	9.5 ± 0.8	71.1 ± 0.3

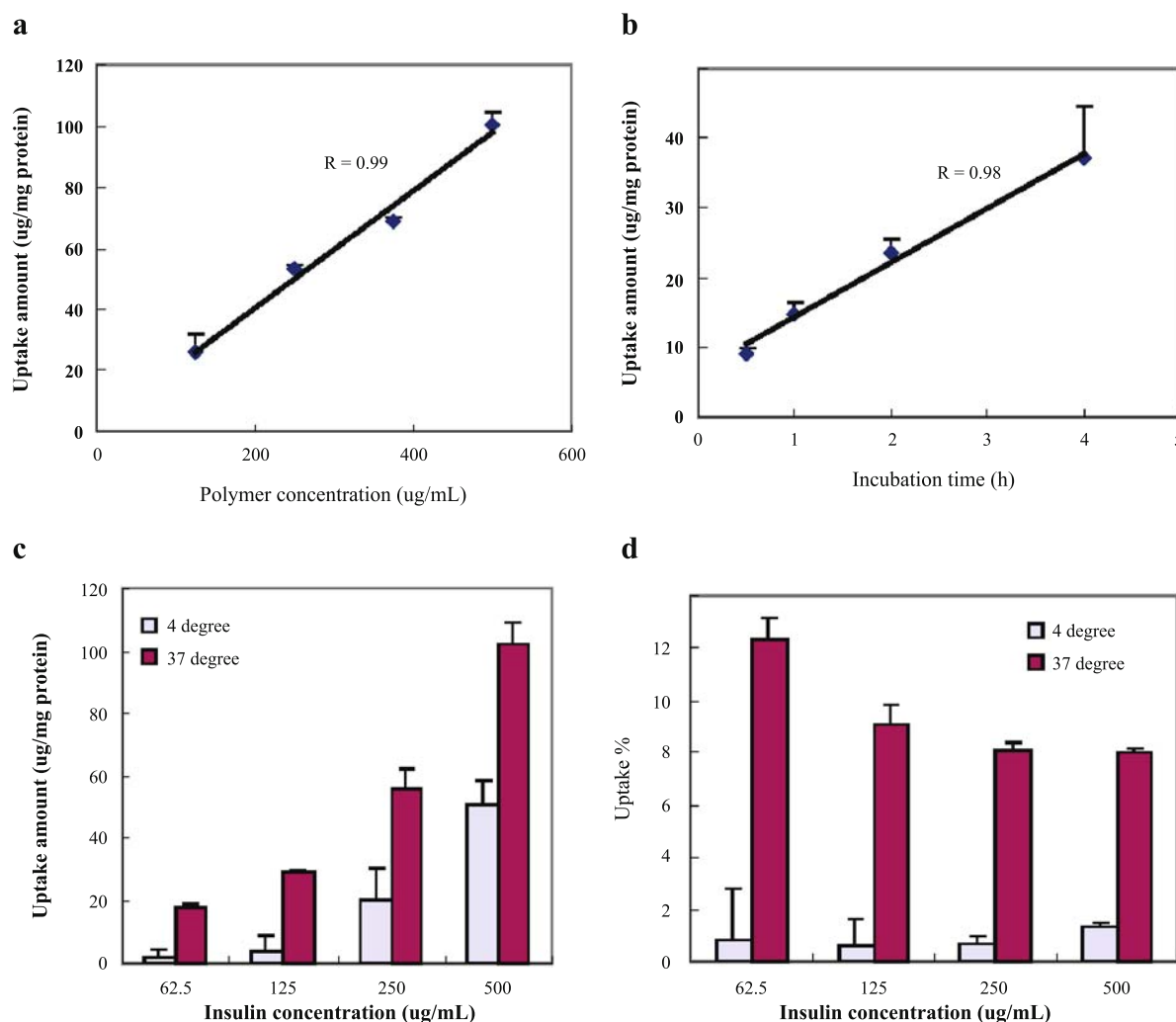


Fig. 2. Effect of polymer concentration, insulin concentration, incubation time, and temperature on complexes uptake in Caco-2 cell line. Error bars represent mean \pm SD ($n = 3$). (a) Effect of PEG(5k)₄₀-g-TMC(100) copolymer concentration on complexes uptake at 37°C. The concentration of insulin was 125 μ g/mL. (b) Effect of incubation time on complex uptake at 37°C. Both the concentration of insulin and PEG(5k)₄₀-g-TMC(100) copolymer used was 125 μ g/mL. (c) Uptake amount vs. insulin concentration. (d) Uptake efficiency vs. insulin concentration.

uptake were reduced by $13.0 \pm 1.0\%$ and $16.6 \pm 0.7\%$, respectively, compared to that of control (Fig. 3). This observation suggests that the complex-induced increase in permeability of insulin was, to some extent, regulated by metabolic energy (cell viability, $p < 0.05$). When the cells were preincubated with 0.1 μ g/mL cytochalasin D, an actin microfilament inhibitor, uptake was decreased by $25.2 \pm 1.3\%$, which is significantly different from that of sodium azide or 2,4-dinitrophenol ($p < 0.05$), implying that uptake may be occurring by adsorptive endocytosis. In contrast, nocodazole, a microtubule inhibitor, caused only a slight reduction in complex uptake of $9.7 \pm 0.5\%$. This is quite reasonable because microtubules are involved in vesicle transport but not in endocytosis (23). Our results are consistent with those reported by Qaddoumi *et al.* (24) on the uptake of 6-coumarin poly (D,L-lactide-co-glycolide) (PLGA) nanoparticles in rabbit conjunctival epithelial cells. In addition, energy depletion was also found to reduce the opening of tight junctions in Caco-2 cells (25). The reduction in complex uptake as a result of energy depletion and

application of endocytosis inhibitors are compatible with adsorptive endocytosis as the main internalization mechanism for insulin complexes in Caco-2 cells.

Visualization by Confocal Laser Scanning Microscopy

To confirm an endocytic uptake mechanism, confocal microscopy was used to provide a direct evidence for complex localization. To distinguish between different cellular structures, cells were double stained with FITC-WGA (membrane, green) and DAPI (blue, nuclei). For uptake and intracellular localization studies of complexes and copolymers, both components were fluorescently labeled. With regard to insulin solution, only a slight reddish fluorescence was observed (Fig. 4D), probably as a result of passive diffusion via the transcellular route. Although there are contradictory reports in the literature concerning the potential of chitosan to be taken up by cells (26), confocal microscopy provided evidence that small amounts of polymers were internalized into Caco-2 cells (Fig. 4C). This is not

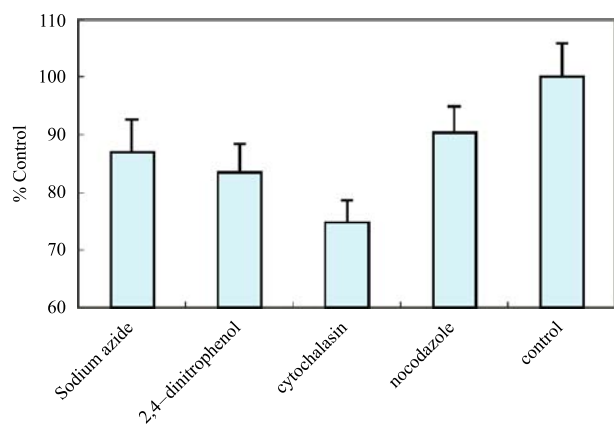


Fig. 3. Effect of energy depletion and vesicle transport inhibitors on PEG(5k)₄₀-g-TMC(100) copolymer-insulin (125 µg/mL) complexes uptake.

surprising because other polycations such as poly-L-lysine and PEI are efficiently internalized by cells (27). In contrast, a significantly higher internalization of cell-associated insulin was found for all investigated complexes compared to the insulin control.

To test whether complexes dissociation occurred upon incubation with the cells, the samples were viewed under confocal microscopy after 2 h incubation. An exemplary image of PEG(5k)₄₀-g-TMC(100)-insulin complexes is shown in Fig. 4A by using blue, red, and green filters, and an overlay of the images showed perfect congruence of red and green dyes. A large amount of yellow color, resulting from the colocalization of green and red, was distributed within the cytoplasm, in small, rounded vesicles localized in the perinuclear area, on the nuclear membrane, and on the apical cell membrane, suggesting that the complexes were internalized into the cells without dissociation. After uptake into the cytoplasm, the complexes might be sorted into endo-/lysosomal compartment. Due to the acidic environment (pH 4.5–5.0) in the endolysosome, both the polymer and insulin are positively charged and the complex will dissociate. Positively charged polymer will interact with the negatively charged vesicle membrane, leading to insulin release. In this case, endolysosomal escape is a rate-limiting step for insulin transport. This could be used to explain the inconsistency that, after 2 h incubation with Caco-2 cells, less complex dissociation was demonstrated by CLSM. In contrast, approximately 80% of insulin was released in acetate buffer pH 4.0 in 2 h.

Moreover, it is well known that chitosan and its derivatives possess mucoadhesive properties. They can attach on the cell surface and cannot be washed away completely. To distinguish between membrane-associated and internalized complexes, trypan blue, a dye that was reported to inhibit extracellular fluorescence (28), was used. An exemplary image is shown in Fig. 4B. Intracellular staining could be clearly observed in the images. Because viable cells excluded trypan blue molecules, the residual fluorescence implied the existence of a substantial amount of intracellular insulin complexes, rather than cell surface adsorption. Interestingly, it was noted that the complexes were mainly localized in the perinuclear region, suggesting endocytic uptake and transport to the lysosomal compartment.

Effect of Polymer Structure on Complexes Uptake in Caco-2 Cells

To study particulate uptake *in vitro*, the most common experimental approach is to use fluorescently labeled particles. Then, particle uptake can be indirectly determined by quantitative extraction of the markers from the cells. Moreover, particles labeled with fluorescent marker also provide visual evidence for cellular uptake. Thus, TRITC-labeled insulin was used in this study.

Here Ca²⁺ and Mg²⁺ were added to the buffer as they are essential for the tight junction function of the cells except for chitosan-insulin complexes, which was unstable in the presence of Ca²⁺/Mg²⁺. In addition, a study was carried out to investigate the effect of buffers with and without Ca²⁺/Mg²⁺, as described in detail in the transport part and no significant influence was found.

To facilitate their direct comparison, all chitosans and copolymers were investigated at 250 µg/mL (constant insulin concentration, 125 µg/mL) except for TMC (125 µg/mL), which is cytotoxic according to MTT assay. TMC displayed an IC₅₀ of approximately 100 µg/mL after 3 h incubation with L929 cells, compared to an IC₅₀ > 500 µg/mL for all the copolymers investigated here. The uptake results after 2 h incubation with Caco-2 cells are shown in Fig. 5. Compared to free insulin solution, all complexes improved insulin uptake significantly ($p < 0.05$), the extent of which depended on the polymer structure. Although the aforementioned study showed that polymer concentration had a significant effect on uptake (Fig. 2), the highest uptake was observed for TMC despite the lower concentration and comparable result was obtained for the copolymer PEG(5k)₄₀-g-TMC(100). With regard to chitosan, insulin uptake efficiency was MW-dependent, and a 2-fold uptake was observed for 100 and 50 kDa chitosan, compared to 400 kDa chitosan. However, an inverse finding was reported by Huang *et al.* (29), who indicated that higher MW is preferable regarding A549 cellular uptake of chitosan nanoparticles. This discrepancy could be explained by the different molecular weight range investigated and different particle size employed. In Huang *et al.*'s report, the range of chitosan molecular weight was 213–10 kDa compared to 400–50 kDa in our study. We assume that the influence of molecular weight depends on whether the molecular weight difference is large enough to cause some changes in PEC parameters. It is well known that cell uptake efficiency was particle size-dependent, and smaller size is preferable (30,31). The decreased particle size (226.8 ± 6.3 vs. 376.4 ± 0.3 for 50 and 400 kDa chitosan, respectively) could probably lead to enhanced uptake. Regarding chitosan at 100 and 50 kDa, it is likely that the molecular weight difference is too small to cause significant influence in complex uptake. In terms of the copolymers, PEG(5k)₄₀-g-TMC(100) (MW = 300 kDa) was more effective compared to PEG(5k)₁₉-g-TMC(50) (MW = 145 kDa) with the same graft ratio. Considering that they have comparable particle size, we assume that besides zeta potential difference (18.8 ± 0.3 vs. 15.0 ± 1.2), polymer molecular weight may play an important role in the permeation ability and high molecular weight is preferred. Ranaldi *et al.* (27) observed a similar phenomenon. Similar results were obtained with PEG(550)₂₂₈-g-TMC(100), PEG(550)₁₃₂-g-TMC(50), and PEG(5k)₁₉-g-TMC(50) copolymers, where uptake quantities were comparable to that of chitosan at 50 kDa.

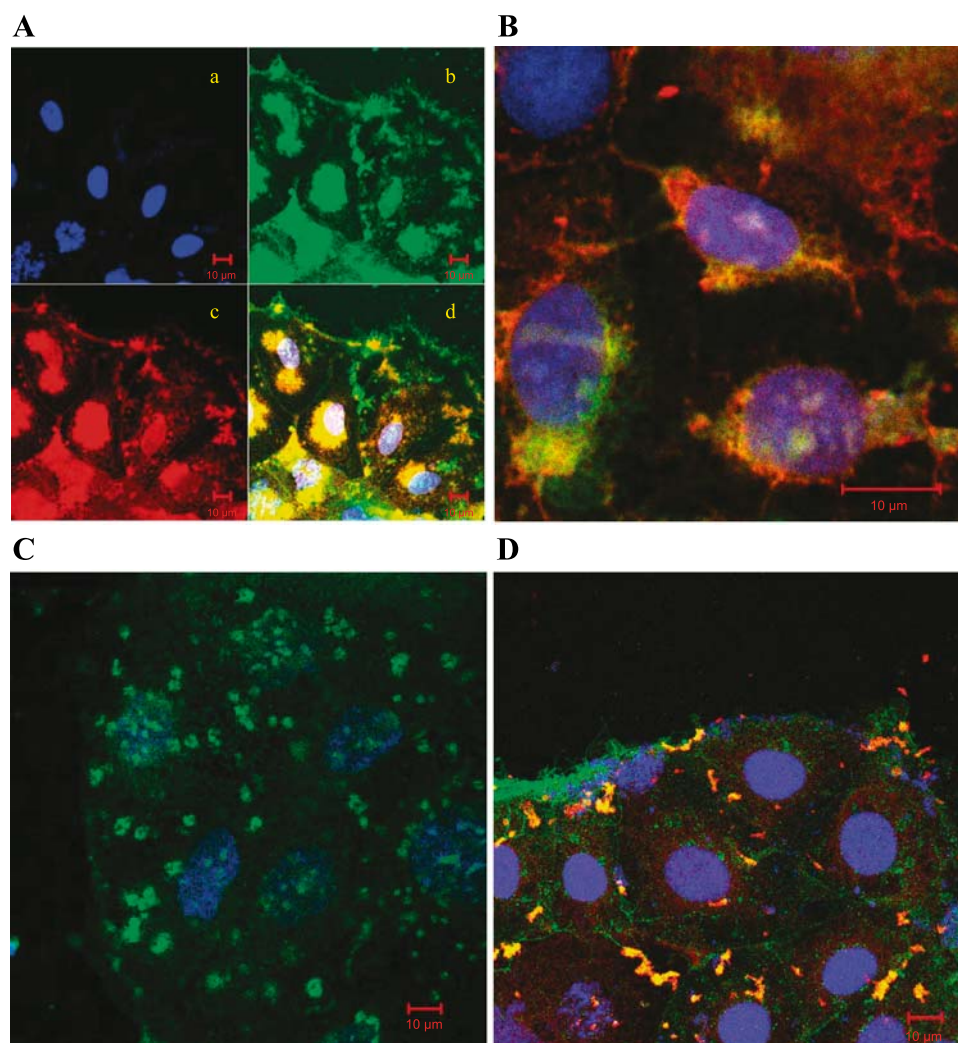


Fig. 4. Confocal micrograph images of Caco-2 cell monolayers incubated with complexes, copolymer, and insulin for 2 h at 37°C. PEG(5k)₄₀-g-TMC(100) copolymer was labeled with Oregon Green 488, insulin was labeled with tetra-methyl-rhodamine isothiocyanate, and nuclei were labeled with 4,6-diamidino-2-phenylindole. (A) Incubated with PEG(5k)₄₀-g-TMC(100) copolymer insulin complexes (a) blue filter, (b) green filter, (c) red filter, (d) overlay of (a)–(c). (B) Incubated with PEG(5k)₄₀-g-TMC(100) copolymer insulin complexes for 2 h and postincubated with trypan blue. (C) Incubated with PEG(5k)₄₀-g-TMC(100) copolymer and postincubated with trypan blue. (D) Incubated with free insulin solution and postincubated with trypan blue. Cell membrane was labeled with fluorescein isothiocyanate-wheat germ agglutinin.

As shown in Fig. 5, complex uptake data were correlated with zeta potential values. The observed high uptake efficiency of 100 and 50 kDa TMC were in line with their high positive charge, and negligible statistical difference was observed between each data set ($p > 0.05$). However, the cytotoxicity of TMC could possibly be a cause for the high uptake efficiency. With similar graft ratios, the cell uptake efficiency of PEG(5k)₄₀-g-TMC(100) insulin complexes, which was comparable to that of pure TMC, was significantly higher than that of PEG(550)₂₂₈-g-TMC(100), probably as a consequence of its relatively high positive charge, whereas the other copolymers had lower zeta potential and showed lower cellular uptake. Nevertheless, negligible statistical difference was observed between PEG(5k)₁₉-g-TMC(50) and PEG(550)₁₃₂-g-TMC(50) insulin complexes ($p > 0.05$).

Transport Studies

Effect of Calcium and Magnesium in the Transport Buffer

The mechanism of chitosan to enhance the absorption of drug substance is reported to be a combination of mucoadhesion and a transient opening of the tight junctions in the mucosal cell membrane (26). The intactness of tight junction is linked to the presence of $\text{Ca}^{2+}/\text{Mg}^{2+}$ ions (32). Reduction of extracellular Ca^{2+} concentration has been reported to result in an opening of tight junctions and consequently increased the paracellular permeability of epithelial cell monolayers (33). Similarly, Ranaldi *et al.* (27) reported that the presence of calcium ions significantly reduced the permeability of Caco-2 cells via treatment with 0.002%

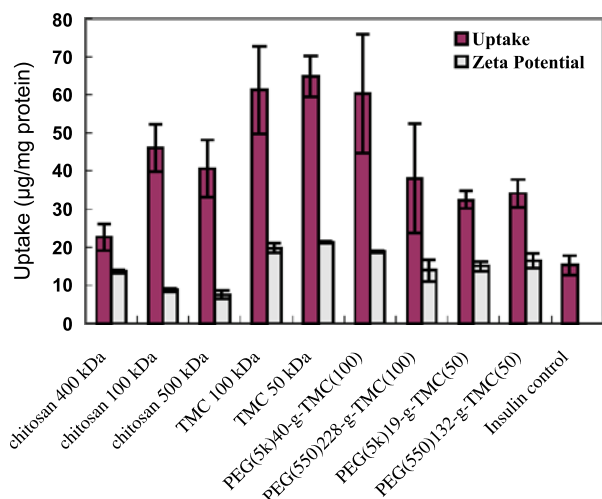


Fig. 5. Uptake of polymer–insulin complexes as a function of polymer structure at 37°C in Caco-2 cell line. Insulin (125 µg/mL) complexes were incubated with cells for 2 h. Error bars represent mean \pm SD ($n = 3$). All chitosans and copolymers were investigated at 250 µg/mL except TMC (125 µg/mL).

chitosan, but had no effect for Mg^{2+} . In contrast, the promoting effect of another polycation, poly-L-arginine, has been demonstrated in a calcium-independent manner (34). The influence of Ca^{2+}/Mg^{2+} on the transport was investigated with PEG(5k)₄₀-g-TMC(100) copolymer–insulin complexes in both cases and their influence was found to be marginal ($p > 0.05$) (Fig. 6a), implying that insulin complexes could not pass through the tight junction, or at least paracellular transport was not the main pathway despite the ability of chitosan derivatives to open the tight junctions. Although tight junctions are dynamic structure and can open and close to a certain degree, when needed, the mean size of the channels is in the order of less than 10 Å, and the transport of large molecules is rather limited. Our previous study also demonstrated this point (21). It showed that after the incubation with a solution of FITC–BSA mixed with chitosan, the detected fluorescence was significantly lower as compared to

chitosan nanoparticles (21). Similarly, if opening the tight junction is the main mechanism, a large amount of insulin should be measured in the basolateral compartment; this, however, is not the case. So far, all data in the literature demonstrated that chitosan derivatives could open the tight junction on a molecular level. No direct evidence was supplied to demonstrate transport of drug substance through a tight junction.

On the other hand, the amount of insulin remaining in the apical compartment after 2 h incubation was measured and the amount of internalized or attached insulin was calculated, as shown in Fig. 6b. Complexes considerably enhanced insulin uptake in Caco-2 cells; approximately 50% of insulin was attached or internalized in the cells, 3.5-fold higher compared with free insulin, irrespective of Ca^{2+}/Mg^{2+} .

Effect of Chitosan MW

Transport of chitosan (100 and 50 kDa)–insulin complexes was investigated in transport buffer without Ca^{2+}/Mg^{2+} , and the P_{eff} values are depicted in Fig. 6a. No significant difference was found between each other ($p > 0.05$), and both of them were considerably lower compared with that of free insulin. Similarly, Ma and Lim (35) reported no measurable level of fluorescence in the basolateral compartment after 4 h incubation with chitosan nanoparticles. Qaddoumi *et al.* (24) also observed a low transport value through cell monolayers with 6-coumarin-loaded nanoparticles. Instead, large amount of insulin complexes (30–50%) were internalized or attached on cell monolayers (Fig. 6b).

Effect of TMC MW in the Copolymers

To elucidate the influence of TMC MW in the copolymers on the transport properties of insulin, two copolymers, PEG(5k)₄₀-g-TMC(100) and PEG(5k)₁₉-g-TMC(50), with similar graft ratio were employed. Results are depicted in Fig. 6. In agreement with the cell uptake results, the P_{eff}

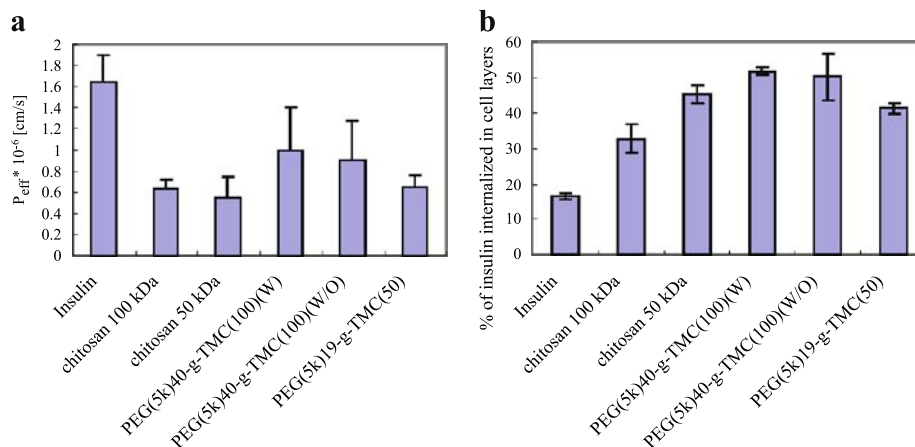


Fig. 6. (a) Apparent permeability coefficient (P_{eff}) of different polymer–insulin nanocomplexes in Caco-2 cells during 120 min ($n = 3$). The concentration of insulin was 250 µg/mL. (b) Percentage of amount of insulin internalized/attached in Caco-2 cell monolayers after 2 h incubation. Each point represents the mean \pm SD of three experiments.

value of PEG(5k)₄₀-g-TMC(100) insulin complexes was higher than that of PEG(5k)₁₉-g-TMC(50), which, however, is not significantly different due to a high standard deviation ($p > 0.05$). PEG(5k)₄₀-g-TMC(100) copolymer is advantageous compared to chitosan concerning transport ($p < 0.05$). No difference was found between PEG(5k)₁₉-g-TMC(50) copolymer and chitosan ($p > 0.05$). Compared to free insulin solution, only at the initial 40 min did PEG(5k)₄₀-g-TMC(100) copolymer–insulin complexes enhance insulin transport remarkably; the difference became marginal after 1 h (data not shown), and the P_{eff} value was slightly lower than the insulin solution ($p > 0.05$). Similar to chitosan–insulin complexes, high internalization could be an advantage of PEC over insulin solution (Fig. 6b).

Additionally, TEER values were measured after 2 h incubation with the complexes. A 40–60% decrease in TEER was measured for the copolymers and these effects were reversible. In contrast, TEER decreased approximately by 60% for 100 and 50 kDa chitosan and no reversibility was observed after 24 h. Ranaldi *et al.* (27) observed the same phenomenon even with 0.01% chitosan. Shortage of calcium and magnesium as a cause could be ruled out, because TEER reversibility was observed after incubation with PEG(5k)₄₀-g-TMC(100) copolymer–insulin complexes in the same buffer. Probably due to the mucoadhesive properties of chitosan, it cannot be washed off completely and the amount left over affects the opening of tight junction.

In Vivo Studies

Based on the uptake and transport data, PEG(5k)₄₀-g-TMC(100) insulin nanocomplexes were selected and the biological efficacy was estimated in diabetic rats by measuring the plasma glucose concentration and compared with that of insulin control solution, as shown in Fig. 7. However, during the 4-h investigation, the decrease in plasma glucose levels was not significantly different from that induced by the insulin control solution ($p > 0.05$). This is in agreement with the results from the transport data in Caco-2 cells, implying that Caco-2 cell line is a reliable *in vitro* cell culture model to predict the absorption of drug substance *in vivo*.

Recently, the pharmacologic response of an insulin–chitosan (MW = 205 kDa, DD = 83%) solution formulation was shown to be significantly larger than those produced by equivalent nanoparticle and complex formulations in the rat and sheep models after intranasal administration (12). There was no significant difference between the pharmacokinetic/pharmacodynamic parameters obtained for the chitosan nanoparticles and complexes compared to insulin control solution (12). This is in agreement with our results. In addition, it should be noted that the pharmacodynamics was investigated at pH 7.4 in our study. It is well known that the absorption enhancing capability of chitosan is pH-dependent, and the effect is more pronounced at pH < 6.5. Additionally, a higher charge density will facilitate the interaction with the nasal mucosa, leading to enhanced absorption. In another study, chitosan (CL110, CL210) nanoparticles (300–400 nm) were shown to increase nasal insulin absorption to a greater extent than insulin control solutions in rabbits (11). However, the experiment was performed at pH 4.3 and the nanoparticles were highly positively charged (11). At any rate, the

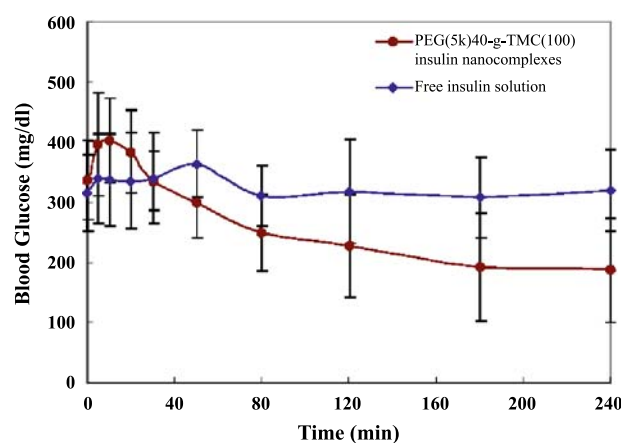


Fig. 7. Hypoglycemic effects of intranasal administration of PEG(5k)₄₀-g-TMC(100) insulin nanocomplexes and control insulin solution. Data represent the mean \pm SD ($n = 4$).

putative advantage of using insulin complexes or nanoparticles for enhancing insulin absorption at physiological pH could not be confirmed. On the other hand, confocal microscopy studies demonstrated that there was still a large amount of insulin complexes available in an intact state within the cells after 2 h incubation. Therefore, the slow release of insulin from the complex might be responsible for the insufficient pharmacological efficiency of the formulation under *in vivo* conditions. In addition, it means that insulin nanocomplexes inside epithelial cell layers will not escape by transcytosis. At present, strategies are being studied to accelerate complex dissociation in the cells. Moreover, mechanisms to activate transcytosis could be promising for further studies.

CONCLUSION

Self-assembled insulin nanocomplexes were formed between insulin and chitosan derivatives. The complexes exhibit a small particle size and high loading efficiency. *In vitro* release of insulin was dependent on the medium pH. Encapsulation of insulin into complexes enhanced association with the Caco-2 cell monolayers up to 3-fold when compared to free insulin solution. The cell uptake efficiency was shown to be a combination of polymer molecular weight, viscosity, and charge density. Uptake of insulin complexes was time-, concentration-, and temperature-dependent. Coincubation with metabolic inhibitors and endocytosis inhibitors prevented complex uptake. Based on studies of uptake and confocal images, internalization of the complexes seems to occur via adsorptive endocytosis, an energy-dependent process occurring by nonspecific interactions of the carrier with the cell membrane, electrostatic interactions between the positively charged complexes and negatively charged membrane, and the mucoadhesive ability of the polymers. However, nanocomplexes did not seem to enhance insulin transport across cell monolayers at physiological pH. This point was further confirmed with *in vivo* data in diabetic rats. The concept of using nanocomplexes for enhancing peptide uptake through epithelia remains controversial. The Caco-2 cell line seems to be a predictive *in vitro* model for studying drug absorption based upon nanocomplexes.

ACKNOWLEDGMENT

Shirui Mao cordially thanks Deutsche Akademische Austauschdienst (DAAD) for the financial support.

REFERENCES

1. A. P. Sayani and Y. W. Chien. Systemic delivery of peptides and proteins across absorptive mucosae. *Crit. Rev. Ther. Drug Carrier Syst.* **13**:85–184 (1996).
2. L. Illum. Nasal drug delivery—possibilities, problems and solutions. *J. Control. Release* **87**:187–198 (2003).
3. R. T. Woodyatt. The clinical use of insulin. *J. Metab. Res.* **2**:793, 1922 (1922).
4. C. McMartin, L. E. Hutchinson, R. Hyde, and G. E. Peters. Analysis of structural requirements for the absorption of drugs and macromolecules from the nasal cavity. *J. Pharm. Sci.* **76**:535–540 (1987).
5. V. H. L. Lee. Protease inhibitors and penetration enhancers as approaches to modify peptide absorption. *J. Control. Release* **13**:213–223 (1990).
6. N. F. Farraj, B. R. Johansen, S. S. Davis, and L. Illum. Nasal administration of insulin using bioadhesive microspheres as a delivery system. *J. Control. Release* **13**:253–261 (1990).
7. F. M. H. M. Merkus, N. G. M. Schipper, W. A. J. J. Hermens, V. S. G. Romeijn, and J. C. Verhoef. Absorption enhancers in nasal drug delivery: efficacy and safety. *J. Control. Release* **24**:201–208 (1993).
8. L. Illum, H. Jorgensen, H. Bisgaard, O. Krogsgaard, and N. Rossing. Bioadhesive microspheres as a potential nasal drug delivery system. *Int. J. Pharm.* **39**:189–199 (1987).
9. K. A. Janes, P. Calvo, and M. J. Alonso. Polysaccharide colloidal particles as delivery systems for macromolecules. *Adv. Drug Deliv. Rev.* **47**:83–97 (2001).
10. L. Illum, I. Jabbal-Gill, M. Hinchcliffe, A. N. Fisher, and S. S. Davis. Chitosan as a novel nasal delivery system for vaccines. *Adv. Drug Deliv. Rev.* **51**:81–96 (2001).
11. R. Fernández-Urrusuno, P. Calvo, C. Remuñán-López, J. Vila-Jato, and M. Alonso. Enhancement of nasal absorption of insulin using chitosan nanoparticles. *Pharm. Res.* **16**:1576–1581 (1999).
12. A. M. Dyer, M. Hinchcliffe, P. Watts, J. Castile, I. Jabbal-Gill, R. Nankervis, A. Smith, and L. Illum. Nasal delivery of insulin using novel chitosan based formulations: a comparative study in two animal models between simple chitosan formulations and chitosan nanoparticles. *Pharm. Res.* **19**:998–1008 (2002).
13. P. Artursson, T. Lindmark, S. S. Davis, and L. Illum. Effect of chitosan on the permeability of monolayers of intestinal epithelial cells (Caco-2 cells). *Pharm. Res.* **11**:1358–1361 (1994).
14. S. Mao, X. Shuai, F. Unger, M. Wittmar, X. Xie, and T. Kissel. Synthesis, characterization and cytotoxicity of poly(ethylene glycol)-graft-trimethyl chitosan block copolymers. *Biomaterials* **26**:6343–6356 (2005).
15. F. Delie. Evaluation of nano- and microparticle uptake by the gastrointestinal tract. *Adv. Drug Deliv. Rev.* **34**:221–233 (1998).
16. S. McClean, E. Prosser, E. Meehan, D. O'Malley, N. Clarke, Z. Ramtoola, and D. Brayden. Binding and uptake of biodegradable poly-DL-lactide micro- and nanoparticles in intestinal epithelia. *Eur. J. Pharm. Sci.* **6**:153–163 (1998).
17. S. Mao, X. Shuai, F. Unger, M. Simon, D. Bi, and T. Kissel. The depolymerization of chitosan: effects on physicochemical and biological properties. *Int. J. Pharm.* **281**:45–54 (2004).
18. M. Simon, M. Wittmar, U. Bakowsky, and T. Kissel. Self-assembling nanocomplexes from insulin and water-soluble branched polyesters, poly[(vinyl-3-(diethylamino)-propylcarbamate-co-(vinyl acetate)-co-(vinyl alcohol)]-graft-poly(L-lactic acid): a novel carrier for transmucosal delivery of peptides. *Bioconjug. Chem.* **15**:841–849 (2004).
19. T. Merdan, K. Kunath, D. Fischer, J. Kopecek, and T. Kissel. Intracellular processing of poly(ethylene imine)/ribozyme complexes can be observed in living cells by using confocal laser scanning microscopy and inhibitor experiments. *Pharm. Res.* **19**:140–146 (2002).
20. E. Walter and T. Kissel. Heterogeneity in the human intestinal cell line Caco-2 leads to differences in transepithelial transport. *Eur. J. Pharm. Sci.* **3**:215–230 (1995).
21. I. Behrens, A. I. V. Pena, M. J. Alonso, and T. Kissel. Comparative uptake studies of bioadhesive and non-bioadhesive nanoparticles in human intestinal cell lines and rats: the effect of mucus on particle adsorption and transport. *Pharm. Res.* **19**:1185–1193 (2002).
22. J. Z. Knaul, S. M. Hudson, and K. A. M. Creber. Improved mechanical properties of chitosan fibers. *J. Appl. Polym. Sci.* **72**:1721–1732 (1999).
23. M. M. Zegers, K. J. Zaal, S. C. van IJzendoorn, K. Klappe, and D. Hoekstra. Actin filaments and microtubules are involved in different membrane traffic pathways that transport sphingolipids to the apical surface of polarized HepG2 Cells. *Mol. Biol. Cell.* **9**:1939–1949 (1998).
24. M. G. Qaddoumi, H. Ueda, J. Yang, J. Davda, V. Labhasetwar, and V. H. L. Lee. The characteristics and mechanisms of uptake of PLGA nanoparticles in rabbit conjunctival epithelial cell layers. *Pharm. Res.* **21**:641–648 (2004).
25. N. G. Schipper, K. M. Varum, and P. Artursson. Chitosans as absorption enhancers for poorly absorbable drugs: 1. Influence of molecular weight and degree of acetylation on drug transport across human intestinal epithelial (Caco-2) cells. *Pharm. Res.* **13**:1686–1692 (1996).
26. N. G. Schipper, S. Olsson, J. A. Hoogstraate, A. G. deBoer, K. M. Vårum, and P. Artursson. Chitosans as absorption enhancers for poorly absorbable drugs: 2. Mechanism of absorption enhancement. *Pharm. Res.* **14**:923–929 (1997).
27. Ranaldi, I. Marigliano, I. Vespiagnani, G. Perozzi, and Y. Sambuy. The effect of chitosan and other polycations on tight junction permeability in the human intestinal Caco-2 cell line. *J. Nutr. Biochem.* **13**:157–167 (2002).
28. C. P. Wan, C. S. Park, and B. H. Lau. A rapid and simple microfluorometric phagocytosis assay. *J. Immunol. Methods* **162**:1–7 (1993).
29. M. Huang, E. Khor, and L.-Y. Lim. Uptake and cytotoxicity of chitosan molecules and nanoparticles: effects of molecular weight and degree of deacetylation. *Pharm. Res.* **21**:344–353 (2004).
30. M. P. Desai, V. Labhasetwar, E. Walter, R. J. Levy, and G. L. Amidon. The mechanism of uptake of biodegradable microparticles in Caco-2 cells is size dependent. *Pharm. Res.* **14**:1568–1573 (1997).
31. T. Jung, W. Kamm, A. Bteitenbach, E. Kaiserling, J. X. Xiao, and T. Kissel. Biodegradable nanoparticles for oral delivery of peptides: is there a role for polymers to affect mucosal uptake? *Eur. J. Pharm. Biopharm.* **50**:147–160 (2000).
32. L. Gonzalez-Mariscal, R. G. Contreras, J. J. Bolivar, A. Ponce, B. Chavez de Ramirez, and M. Cerejido. Role of calcium in tight junction formation between epithelial cells. *Am. J. Physiol.* **259**:C978–C986 (1990).
33. A. B. J. Noach, Y. Kurosaki, M. C. M. Blom-Rosmalen, A. G. de Boer, and D. D. Breimer. Cell-polarity dependent effect of chelation on the paracellular permeability of confluent Caco-2 cell monolayers. *Int. J. Pharm.* **90**:229–237 (1993).
34. K. Ohtake, T. Maeno, H. Ueda, M. Ogihara, H. Natsume, and Y. Morimoto. Poly-L-arginine enhances paracellular permeability via serine/threonine phosphorylation of ZO-1 and tyrosine dephosphorylation of occludin in rabbit nasal epithelium. *Pharm. Res.* **20**:1838–1845 (2003).
35. Z. Ma and L. Lim. Uptake of chitosan and associated insulin in Caco-2 cell monolayers: a comparison between chitosan molecules and chitosan nanoparticles. *Pharm. Res.* **20**:1812–1819 (2003).